


Simulating chiral spin liquids with fermionic projected entangled pair states

Sasank Budaraju^{1,2,*}, Didier Poilblanc^{1,†} and Sen Niu^{1,3,‡}

¹*Laboratoire de Physique Théorique, Université de Toulouse, CNRS, 31400 UPS, France*

²*Department of Physics and Quantum Centre of Excellence for Diamond and Emergent Materials (QuCenDiEM), Indian Institute of Technology Madras, Chennai 600036, India*

³*Department of Physics and Astronomy, California State University Northridge, California 91330, USA*

 (Received 15 March 2024; revised 4 June 2024; accepted 9 July 2024; published 2 August 2024)

Chiral spin liquids (CSL) based on spin-1/2 fermionic projected entangled pair states (fPEPS) are considered on the square lattice. First, fPEPS approximants of Gutzwiller-projected Chern insulators (GPCI) are investigated by variational Monte Carlo (VMC) techniques on finite-size tori. We show that such fPEPS of finite bond dimension can correctly capture the topological properties of the chiral spin liquid, as the exact GPCI, with the correct topological ground-state degeneracy on the torus. Further, more general fPEPS are considered and optimized (on the infinite plane) to describe the CSL phase of a chiral frustrated Heisenberg antiferromagnet. The chiral modes are computed on the edge of a semi-infinite cylinder (of finite circumference) and shown to follow the predictions from conformal field theory. In contrast to their bosonic analogs the (optimized) fPEPS do not suffer from the replication of the chiral edge mode in the odd topological sector.

DOI: [10.1103/PhysRevB.110.064402](https://doi.org/10.1103/PhysRevB.110.064402)

I. INTRODUCTION

Commonly, a quantum spin liquid refers to a quantum state that does not break spontaneously the system symmetries, neither the space group symmetry nor the global continuous [e.g., $SU(2)$] symmetry, if any of those is present in the Hamiltonian. In particular, spin liquids show absence of magnetic ordering down to zero temperature. Chiral spin liquids (CSLs) are exotic states of matter characterized, in addition to their spin liquid character, by the breaking of time-reversal (T) and parity (P) symmetries [1]. They also exhibit long-range topological order [2]. They have been encountered in several quantum spin models with $SU(2)$ [3–10] or higher $SU(N)$ [11–18] symmetry in the presence of a chiral term breaking explicitly T and P . In some cases, P and T can be broken spontaneously, as demonstrated in both Hubbard-/Heisenberg-like models [19–26] and Kitaev models [27] on lattices with odd plaquettes [28–35]. Parent Hamiltonians have also been devised for CSLs [36–38].

Experimental efforts to identify compounds with CSL ground states are ongoing, with prominent attention devoted to spin-orbit coupled materials with Kitaev-like interaction under external magnetic fields [39–41]. Additionally, in Moiré heterostructures, the layer degree of freedom regarded as a pseudospin facilitates realization of pseudochiral spin liquids [42]. Chiral spin liquids have also been proposed in cold atom platforms using Floquet driving [43] or Rydberg arrays [44–47] where the chirality of edge modes can be detected experimentally. CSLs relevant for Rydberg atom

models on the honeycomb lattice have recently been classified via a projective symmetry group approach [48].

As CSLs typically emerge in strongly correlated systems, numerical tools for determining phase diagrams of generic Hamiltonians and characterizing CSLs are desired. Tensor networks such as projected entangled pair states (PEPS) [49] are well suited to the investigation of spin liquids. Topological orders can be encoded naturally by imposing virtual gauge symmetries [50,51]. In addition, chiral forms of PEPS can describe CSL [52,53] and be used as an efficient variational scheme to attack frustrated quantum spin models hosting CSL phases [54,55]. On the other hand, infinite PEPS (iPEPS) is an ideal tool as it defines states in the thermodynamic limit directly, avoiding finite-size extrapolations.

Despite the above-mentioned successes and strengths of the PEPS framework, it has remained challenging to figure out completely whether conventional bosonic PEPS can truly describe CSL. In particular, it is still unclear whether topological obstruction [56,57] affects, in addition to small artifacts in the long distance real-space correlations (presence of a gossamer tail [54,58]), global topological properties such as (i) the topological GS degeneracy or (ii) the correct conformal field theory (CFT) counting in the entanglement spectrum (ES). For the nonchiral case, PEPS is believed to be a conceptually good *Ansatz*, topological order being encoded by gauge symmetry [51,59]. In contrast, whether chiral PEPS give the correct topological degeneracy of the CSL is still unsettled in general due to expensive computation cost [52], except in very rare cases where bond dimension is very small [60]. For example, in the case of the $SU(2)_1$ CSL, although one can insert string (Wilson loop) operators in x and/or y directions, the resulting states are not linearly independent and the degeneracy should be only 2, which has not been definitely proven in chiral (bosonic) PEPS (although results are not

*Contact author: budaraju@irsamc.ups-tlse.fr

†Contact author: didier.poilblanc@irsamc.ups-tlse.fr

‡Contact author: sen.niu@irsamc.ups-tlse.fr

inconsistent with that claim) [52]. In addition, simple chiral PEPS revealed a doubling of the chiral edge branch in the odd topological sector [52,53], which seems to persist in the case of fully optimized wave functions for Abelian $SU(N)_1$ and non-Abelian CSLs [11,14,54,55,58,61].

In this paper, based on the recently proposed projected fermionic PEPS (fPEPS) *Ansatz*, we show, using VMC techniques, that PEPS can represent CSLs with correct topological degeneracy. Using this fPEPS *Ansatz* as initial state, we further perform variational optimization to attack a frustrated $J_1 - J_2 - J_\chi$ square lattice model [62] in the regime of chiral spin liquid [54,63,64]. The fPEPS approach has competitive energy compared to the conventional bosonic PEPS, and crucially shows correct ES degeneracy.

The rest of this paper is structured as follows. In Sec. II, we discuss the numerical techniques employed, including the construction of the parton *Ansatz* and the VMC and PEPS methods. Then, in Sec. III we show results of the VMC analysis of fPEPS states on finite clusters, and in Sec. IV we discuss the variational optimization of the fPEPS states on the infinite plane to study the $J_1 - J_2 - J_\chi$ model.

II. NUMERICAL TECHNIQUES

A. Parton ansatz

In order to construct a simple CSL, we first consider a Chern insulator state with $C = 1$, obtained by diagonalizing the following (free electron) Hofstadter Hamiltonian on the square lattice

$$H = \sum_{\langle ij \rangle, \sigma} t_1 \chi_{ij} c_{i\sigma}^\dagger c_{j\sigma} + \sum_{\langle\langle ik \rangle\rangle, \sigma} t_2 c_{i\sigma}^\dagger c_{k\sigma} e^{i\theta_{ik}} + \text{H.c.}, \quad (1)$$

where $\langle ij \rangle$ ($\langle\langle ik \rangle\rangle$) denotes nearest (next-nearest)-neighbor bonds and σ is the spin index, $\sigma = \{\uparrow, \downarrow\}$. The hoppings are identical for both spin species. We fix $t_2 = 0.5t_1$, $\chi_{ij} = \pm 1$ to ensure a π flux through every square plaquette and choose the complex phases θ_{ik} to obtain a $\pi/2$ flux in all triangles. In this paper we choose the gauge used in Ref. [65] such that the unit cell can be chosen as two nearest-neighbor sites along the x direction.

The exact many-body spin wave function $|\varphi\rangle$ is a Gutzwiller projected Slater-determinant

$$|\varphi\rangle = P_G \prod_{\alpha} c_{\alpha, \uparrow}^\dagger c_{\alpha, \downarrow}^\dagger |0\rangle, \quad (2)$$

where the Gutzwiller-projector $\prod_i (n_{i, \uparrow} - n_{i, \downarrow})^2$ projects onto the subspace of exactly one electron per site, and $c_{\alpha, \sigma}^\dagger$ correspond to single-particle states obtained from the mean-field Hamiltonian Eq. (1). For Gaussian fPEPS, the set of $c_{\alpha, \sigma}^\dagger$ orbitals are only represented approximately due to truncation of finite bond dimension. Details on Gaussian fPEPS will be provided in Sec. II B.

It is known that the resultant exact parton state is a $SU(2)_1$ CSL, which is equivalent to the $\nu = 1/2$ bosonic Laughlin state. On a torus, such CSL has twofold topological degeneracy where the degenerate states can be constructed by imposing different boundary conditions on the parton wave functions [66]. On a cylinder, the CSL hosts chiral gapless edge states predicted by $SU(2)_1$ Wess-Zumino-Witten

(WZW) CFT. In the rest of our work, we dub this parton state in (2) the exact CSL, in contrast to its fPEPS approximation to be discussed below.

B. Construction of Gaussian fPEPS state

To construct the Gaussian fPEPS state, which is an approximation of the exact ground state of Eq. (1), we adopt the method introduced in Refs. [67,68]. The translation invariant many-body *Ansatz* is parametrized by a single Gaussian tensor with four virtual indices and two physical indices corresponding to the unit cell in the Hofstadter model. In the Gaussian tensor, the virtual space dimension is defined by the number of virtual modes M . Each virtual fermion mode can be occupied or unoccupied, thus the bond dimension becomes $D = 2^M$ for a spinless state and $D = 4^M$ for spinful $SU(2)$ state. To obtain the best approximation of the Gaussian fPEPS tensor, we use gradient optimization and choose the (free electron) energy of Eq. (1) at half-filling as cost function.

As the unprojected fPEPS state is Gaussian, it can be also written as a Slater determinant (product state) on any finite torus and all the physical properties can be extracted exactly. In Ref. [65] it has been shown that the unprojected fPEPS becomes chiral from $M \geq 2$, and the correlation functions improve quantitatively with increasing M . However, general topological properties of the fPEPS remain unclear after Gutzwiller projection, and are not accessible (except for the ES) by conventional PEPS techniques. Hence we introduce the following Monte Carlo method to probe the properties of Gutzwiller projected Gaussian fPEPS.

C. Monte Carlo technique

The Gutzwiller projected fPEPS wave functions discussed previously are analyzed within a standard Markov chain Monte Carlo framework [69]. In particular, overlaps between two projected wave functions $|\psi\rangle$ and $|\phi\rangle$ can be computed straightforwardly as follows,

$$\frac{\langle \psi | \phi \rangle}{\langle \psi | \psi \rangle} = \frac{\sum_x \langle \psi | x \rangle \langle x | \phi \rangle}{\langle \psi | \psi \rangle} = \frac{\sum_x |\langle \psi | x \rangle|^2 \frac{\langle x | \phi \rangle}{\langle x | \psi \rangle}}{\langle \psi | \psi \rangle}, \quad (3)$$

where $\{|x\rangle\}$ is chosen to be the S_z basis to enforce the one fermion per site constraint exactly. In this paper, we remain in the $S_z = 0$ sector, with equal number of up and down spins. Then, by sampling the normalized probability distribution

$$P(x) = \frac{|\langle \psi | x \rangle|^2}{\langle \psi | \psi \rangle} \quad (4)$$

one can estimate the wave-function overlap as

$$\frac{\langle \psi | \phi \rangle}{\langle \psi | \psi \rangle} \sim \frac{1}{n} \sum_{i=1}^n \frac{\langle x_i | \phi \rangle}{\langle x_i | \psi \rangle}, \quad (5)$$

where n is the number of Monte Carlo runs, and $\{|x_i\rangle\}$ are the spin configurations sampled in the Markov chain. We note that the cost of computing overlaps for the projected fPEPS is independent of bond dimension, as the set of single-particle orbitals in real space can be obtained analytically for any M . This enables the calculations in Sec. III, where we quantitatively analyze the fPEPS for $M = 1 \dots 6$.

D. Variational iPEPS method

In Sec. IV, we perform a variational study of the chiral Heisenberg antiferromagnetic model, taking the projected fPEPS parton *Ansatz* as the initial state in our optimization. First, we construct the Gutzwiller projected tensor for parton *Ansatz* following Refs. [65,68], where a single tensor of bond dimension 4^M contains two physical sites and satisfies $U(1) \times SU(2)$ symmetry. Second, we choose this tensor as initial state and variationally optimize the tensor elements with the $U(1) \times SU(2)$ virtual symmetry kept. To optimize the tensor, we adopt the automatic difference method [70] and choose the energy of the chiral spin model as the cost function. The energy is evaluated from the corner transfer matrix renormalization group (CTMRG) [71,72] method, where the approximate contraction is controlled by the environment bond dimension χ , and becomes exact in the $\chi \rightarrow \infty$ limit.

III. CHARACTERIZATIONS OF PROJECTED fPEPS PARTON ANSATZ: VMC STUDIES

Several VMC algorithms have been developed to study topological properties of spin liquids, including entanglement entropy, modular matrices, and topological degeneracy [66,73,74]. In this section, using VMC calculations on finite tori, we investigate the properties of the fPEPS wave functions, and compare them to the exact CSL state constructed from the parton *Ansatz* (2). We demonstrate that the fPEPS at finite bond dimension can capture the correct properties of the CSL. The Gaussian fPEPS tensor is determined from optimizing the mean-field Hamiltonian (1) on a 80×80 torus. Subsequently, we put the optimized tensor on smaller $L \times L$ clusters to construct the many-body wave functions, which are input to the Monte Carlo algorithm.

A. Wave function fidelity

We first compute the normalized overlap between the projected exact CSL and the fPEPS states with periodic boundary conditions (PBC-PBC), given by

$$O_M = \frac{|\langle \Psi_{\text{exact}} | \Psi_M \rangle|}{\sqrt{\langle \Psi_{\text{exact}} | \Psi_{\text{exact}} \rangle \langle \Psi_M | \Psi_M \rangle}}. \quad (6)$$

By contracting physical indices of the PEPS, the overlap can be mapped to a partition function of a two-dimensional classical statistical model, thus decaying exponentially with system size. We can then define the fidelity per unit area (free energy) $f = (O_M)^{1/L^2}$, which should show weak size dependence and converge to a finite value in the $L \rightarrow \infty$ limit. The infidelity $1 - f$ plotted in Fig. 1 confirms these expectations. In addition, the diminishing infidelity with increasing M clearly demonstrates the improving accuracy of the optimized fPEPS states. We note that similar results have been obtained for the other three choices of boundary conditions, i.e., PBC-APBC, APBC-PBC and APBC-APBC.

B. Spin-spin correlations

To further confirm that the projected fPEPS describe the correct physical properties of the CSL, we compute the real-space spin-spin correlations for the $L = 18$ system, shown in

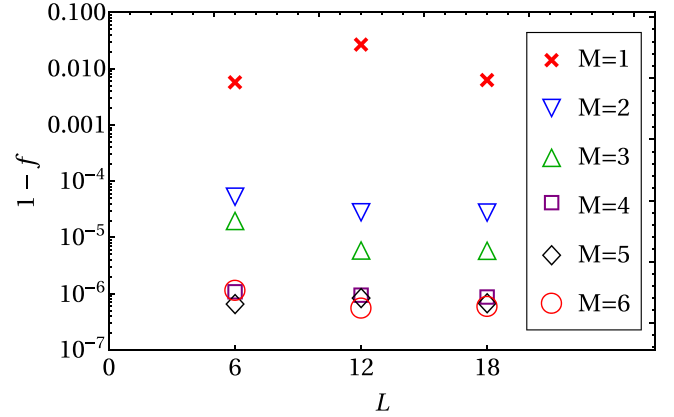


FIG. 1. Infidelity $1 - f$ plotted in logarithmic scale as a function of the system size L for fPEPS states with $M = 1 \dots 6$ and periodic boundary conditions. The estimated error bars are smaller than the size of the symbols.

Fig. 2. We observe exponential behavior at short distances as expected for a gapped state, with a very short correlation length $\xi \approx 0.57$. Further, the fPEPS states (for all values of M) are essentially indistinguishable from the exact CSL in terms of the correlations. Note that the saturation of the decay of the long-distance correlations for $r > 5$ can be simply attributed to a finite-size effect with periodic boundary conditions when $r \sim L/2$. Hence, we cannot definitively establish the presence of a gossamer tail, an artifact due to the bulk-boundary correspondence that has been discussed in several previous works [58,61,65].

C. Topological properties: Ground-state degeneracy

A fundamental characteristic of a topological ordered phase is a ground-state degeneracy, which depends on the topology of space [75]. As mentioned previously, the

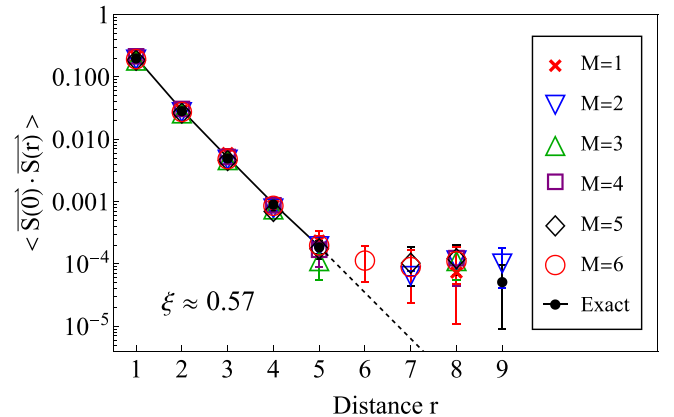


FIG. 2. Logarithmic plot of the magnitude of spin-spin correlations as a function of distance for the exact CSL and projected fPEPS, for the $L = 18$ cluster with periodic boundary conditions. Symbols are omitted if the obtained value is lesser than one standard deviation of error. The expected correlations of the exact CSL at $r > 5$ (in the thermodynamic limit) are shown as a dotted line, extending the exponential behavior.

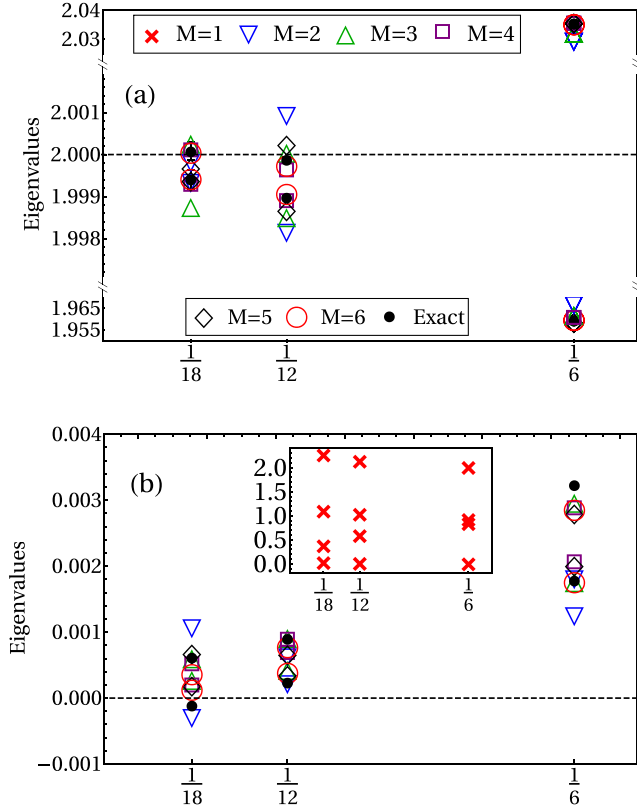


FIG. 3. Eigenvalues of the overlap matrix as a function of inverse system size $1/L$ for the exact and the fPEPS states. Pairs of eigenvalues converge to $+2$ and 0 in (a) and (b), respectively. The $M = 1$ data is shown in the inset since it has a much larger deviation than the other fPEPS states. The estimated error bars are roughly the size of the symbols.

exact $SU(2)_1$ CSL state (2) has a twofold degeneracy on a torus: imposing different boundary conditions on the parton *Ansatz* before projection yields degenerate states that cannot be distinguished by local observables (such as spin-spin correlations) after projection. In the thermodynamic limit the four states only span a two-dimensional linear space [66].

To investigate this property of the fPEPS and exact states on finite clusters, we compute the 4×4 overlap matrix O with elements

$$O_{\alpha,\beta} = \frac{\langle \Psi_M^\beta | \Psi_M^\alpha \rangle}{\sqrt{\langle \Psi_M^\alpha | \Psi_M^\alpha \rangle \langle \Psi_M^\beta | \Psi_M^\beta \rangle}}, \quad (7)$$

where α and β denote the four choices of boundary conditions on the torus. The rank of this Hermitian matrix (which denotes the number of linearly independent eigenvectors) is the number of nonzero eigenvalues. In the thermodynamic limit, the eigenvalues of the exact state must converge to $\{+2, +2, 0, 0\}$ (the trace of the matrix being 4). In Fig. 3, we plot the eigenvalues for both the projected fPEPS and the exact states as a function of L . Remarkably, we observe that for fixed $M > 1$, the eigenvalues converge to the exact result with increasing system size (already at $L = 18$, the deviation is at most 10^{-3}). In addition, from the analysis of the eigenvectors of the overlap matrix, we have obtained the following relations

(up to a gauge degree of freedom):

$$\begin{aligned} |\Psi^{\text{PBC-PBC}}\rangle &= \frac{|\Psi^{\text{PBC-APBC}}\rangle + |\Psi^{\text{APBC-PBC}}\rangle}{\sqrt{2}}, \\ |\Psi^{\text{APBC-APBC}}\rangle &= \frac{|\Psi^{\text{PBC-APBC}}\rangle - |\Psi^{\text{APBC-PBC}}\rangle}{\sqrt{2}} \end{aligned} \quad (8)$$

with a very good accuracy whenever $L \geq 18$, consistent with the fact that the states on the right-hand side and the left-hand side of the above equations belong to the same IRREPs of the C_4 rotation group on clusters with $L_x = L_y$ (respectively, even and odd). These results substantiate that fPEPS, even at finite bond dimensions, can accurately capture the correct topological degeneracy of CSL states. This is one of the main results of our work.

IV. SIMULATION OF THE CHIRAL $J_1 - J_2 - J_\chi$ MODEL

From the VMC analysis in the previous section, we have seen that projected (Gaussian) fPEPS can describe topological properties of CSL faithfully. However, for the purpose of studying frustrated spin models, the conventional parton *Ansatz* has limited number of variational parameters such as hopping coefficients, Jastrow factors, etc. On the contrary, PEPS can represent generic interacting states with the systematic increase of bond dimension. Now we conduct a variational PEPS study on the chiral $J_1 - J_2 - J_\chi$ model using projected GfPEPS as the initial *Ansatz*. The spin-1/2 Hamiltonian is given by

$$\mathcal{H} = J_1 \sum_{\langle i,j \rangle} \mathbf{S}_i \cdot \mathbf{S}_j + J_2 \sum_{\langle\langle i,k \rangle\rangle} \mathbf{S}_i \cdot \mathbf{S}_k + J_\chi \sum_{\Delta_{ijk}} (\mathbf{S}_i \times \mathbf{S}_j) \cdot \mathbf{S}_k. \quad (9)$$

This model was initially proposed in Ref. [62], where exact diagonalization techniques revealed that the ground state had a very high overlap with the exact Kalmeyer-Laughlin state. The model exhibits a chiral spin liquid (CSL) phase over a large region of its phase diagram, and we select a specific set of parameters also discussed in that work. The Hamiltonian can be understood as an effective Hamiltonian of the Fermi-Hubbard model through the Schrieffer-Wolff transformation. Realizing the Fermi-Hubbard model in cold atom experiments remains an active area of research [76–78]. Further, this model has been investigated in Ref. [54], where the sum of four triangular J_χ terms inside a plaquette has been equivalently written as a spin cyclic permutation $i(P_{ijkl} - P_{ijkl}^{-1})$ term. Reference [54] performed a variational study of this model with bosonic iPEPS, and found a regime of $SU(2)_1$ CSL in the phase diagram. The optimized bosonic iPEPS provides good variational energy and correct level counting in the ES predicted by $SU(2)_1$ WZW CFT. However, there exists a redundant chiral branch in the odd (semion) sector [54,79], which contradicts both the theoretical prediction and recent numerical results obtained from DMRG on finite cylinders [63,64]. We emphasize that such artificial replication of chiral branches in bosonic iPEPS is quite general and is also found in the cases of $SU(N)$ and non-Abelian CSLs [11,14,55,61].

On the other hand, in Ref. [65] it was shown that the projected fPEPS from parton construction not only has correct

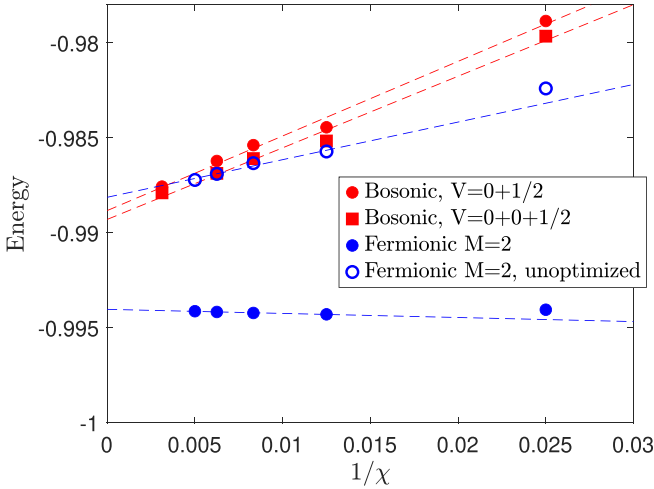


FIG. 4. Variational energy of optimized bosonic iPEPS (red) and projected fermionic iPEPS (blue) for the spin model. Blue open circle shows the energy of the fermionic parton *Ansatz* at $t_1 = 1, t_2 = 0.5$ without variational optimization of tensor elements.

level counting, but also has exact branch numbers in each topological sector of the ES. However, it is not clear whether such ES degeneracy of fPEPS is a robust or fine-tuned feature. From the variational study below we would like to show that (i) the parton state provides an energetically good initial guess for variational optimization and (ii) the optimized fPEPS state (which is beyond projected Gaussian states) still gives the correct ES counting and number of chiral modes, implying that our family of fPEPS states is not fine tuned and provides a faithful description of CSLs.

A. Variational energy

We choose the parameters of the spin model as $J_1 = 2 \cos(0.06\pi) \cos(0.14\pi)$, $J_2 = 2 \cos(0.06\pi) \sin(0.14\pi)$, $J_\chi = 4 \sin(0.06\pi)$, which has been considered in Refs. [54,58,62] and is known to be deep inside the CSL phase with the ground-state energy being $E \approx -1$. We import the SU(2) bosonic iPEPS method there and compute variational energies as a reference. For the bosonic iPEPS, the tensor has SU(2) symmetry and the unit-cell size is chosen to be one such that each tensor only has one physical leg. The results for virtual spaces $V = 0 \oplus 1/2$ ($D = 3$) and $V = 0 \oplus 0 \oplus 1/2$ ($D = 4$) are given in Fig. 4. As we extrapolate to the infinite χ limit the energies are around -0.99 .

In our fPEPS treatment, the initial parton state is still chosen at the hopping parameter $t_1 = 2t_2$, which corresponds to the largest band gap. Since the smallest bond dimension $M = 1$ is nonchiral, we take $M = 2$ ($D = 16$) GfPEPS with Gutzwiller projection and compute the energy with respect to the spin model. Due to the gauge choice in the parton construction, the smallest unit-cell size is two sites along x direction. As can be seen in Fig. 4, the unoptimized parton state already has good energy close to the optimized bosonic iPEPS at $D = 3, 4$. After optimizing the fPEPS tensor elements, the energy further improves to $E \approx -0.995$. When comparing the energies of bosonic and fermionic iPEPS, one should recall

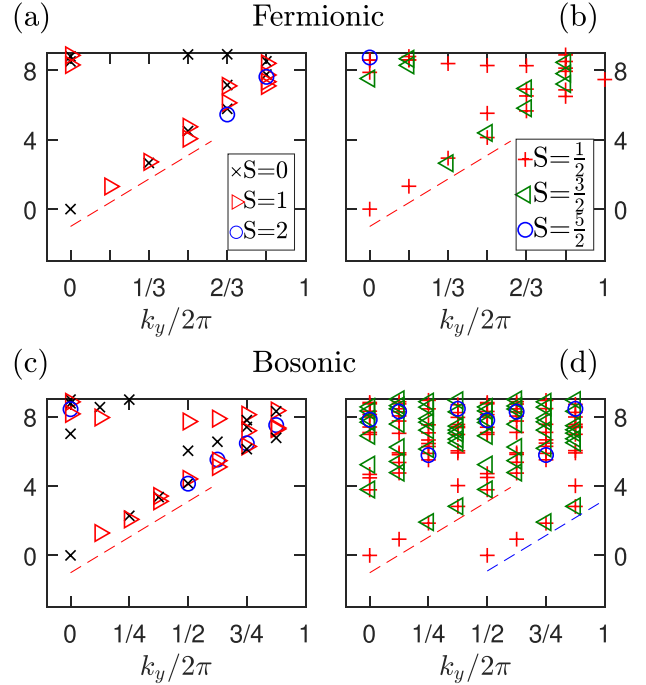


FIG. 5. ES of optimized $M = 2$ projected fermionic iPEPS (top) and $D = 3$ bosonic iPEPS (bottom) for the spin model on cylinders of finite width 6 and 8, respectively. Left and right columns correspond to even (integer spin) and odd (half-integer spin) sectors. The red dashed lines denote the theoretically predicted linear dispersions of the tower of states, while the blue dashed line denotes the redundant branch in the odd sector of bosonic iPEPS.

that since our fPEPS has two-sites unit cell in y direction, the effective bond dimension in y direction is $D_{\text{eff}} = 4$ per site, while the x direction bond is much larger than that of bosonic iPEPS. This is consistent with the fact that our fermionic iPEPS has better energy.

B. Entanglement spectrum

Aside from modular matrices, bulk topology of CSLs can also be characterized by edge (entanglement) spectrum according to bulk-boundary correspondence. To analyze the level counting of ES, we put our optimized tensor on a finite width cylinder and compute the ES of such translation-invariant state. To compute ES, the boundary Hamiltonian (transfer matrix fixed points) can be constructed exactly by exact contraction [80] or approximately by grouping CTMRG environment T tensors [53]. In the case of fermionic iPEPS, the tensor has $U(1) \times SU(2)$ virtual symmetry and the transfer matrix fixed points are labeled by virtual charge and parity of virtual spin, while in the case of bosonic iPEPS the tensor only has SU(2) virtual symmetry and the transfer matrix fixed points are labeled only by parity of virtual spin. Figures 5(a)–5(b) show ES of optimized $M = 2$ fermionic iPEPS computed from CTMRG with $\chi = 110$. The low-energy spectrum shows SU(2) multiplets with counting $0, 1, 0 + 1, 0 + 1 + 1, \dots$, in the integer spin sector and $1/2, 1/2, 1/2 + 3/2, \dots$, in the half-integer spin sector, satisfying prediction from $SU(2)_1$ WZW CFT. Note that in both even and odd sectors there is

only one low-energy chiral branch, which matches with recent DMRG results on finite cylinders [63,64]. On the contrary, Figs. 5(c)–5(d) show ES of $D = 3$ bosonic iPEPS where the level counting is correct but an anomalous identical branch appears in the odd sector with a π -momentum shift. We also confirmed that the redundant branch can not be eliminated or shifted by increasing the bond dimension of the bosonic iPEPS. In future works, it would be interesting to see whether such artifact of bosonic iPEPS can be eliminated by further imposing virtual $U(1)$ symmetry and/or increasing the unit-cell size like in the fPEPS case.

V. CONCLUSION AND OUTLOOK

Tensor network methods have been widely applied to study frustrated spin models hosting possible spin liquid phases. However, due to a no-go theorem [57], doubts have arisen regarding their ability to describe chiral spin liquid states. In this work, we investigated the topological properties of projected fPEPS *Ansatz* for a CSL state. By performing a VMC analysis on the initial parton state, we demonstrated that fPEPS at finite bond dimension can accurately capture the topological GS degeneracy of CSLs. This achievement has been challenging with conventional bosonic PEPS due to the high computational cost involved [52]. Additionally, our results show that the fPEPS *Ansatz* effectively captures the spin-spin correlation functions of the CSL. Given the high

quality of overlap fidelity, we anticipate that fPEPS will also accurately reproduce the modular S and T matrices.

Further, non-Gaussian fPEPS *Ansätze* were optimized variationally for the $J_1 - J_2 - J_\chi$ Heisenberg model and were found to have competitive energy compared to their bosonic counterparts, while retaining the correct level counting of the entanglement spectrum as opposed to bosonic iPEPS, which have a duplicate branch in the odd topological (semion) sector.

Our work provides further supporting evidence for using PEPS methods in describing topologically ordered states. For example, fPEPS *Ansätze* can further be used to study fermionic Hofstadter-Hubbard model [81] where both the Chern insulating phase and CSLs can be tuned by varying the strength of Hubbard interaction (e.g., Ref. [42]). In that case, our Gaussian fPEPS *Ansätze* with partially projected doublons are expected to be good initial variational *Ansätze* at finite Hubbard interaction.

ACKNOWLEDGMENTS

We thank F. Becca and Y. Iqbal, for discussions on VMC, as well as J.-W. Li and J.-Y. Chen. S.B. acknowledges financial support from the Indo-French Centre for the Promotion of Advanced Research - CEFIPRA Project No. 64T3-1. D.P. acknowledges support from the TNTOP ANR-18-CE30-0026-01 grant awarded by the French Research Council. This work was granted access to the HPC resources of CALMIP center under allocations 2023-P1231 and 2024-P1231.

-
- [1] X. G. Wen, F. Wilczek, and A. Zee, Chiral spin states and superconductivity, *Phys. Rev. B* **39**, 11413 (1989).
 - [2] X.-G. Wen, Gapless boundary excitations in the quantum Hall states and in the chiral spin states, *Phys. Rev. B* **43**, 11025 (1991).
 - [3] B. Bauer, L. Cincio, B. P. Keller, M. Dolfi, G. Vidal, S. Trebst, and A. W. Ludwig, Chiral spin liquid and emergent anyons in a kagome lattice Mott insulator, *Nat. Commun.* **5**, 5137 (2014).
 - [4] A. Wietek and A. M. Läuchli, Chiral spin liquid and quantum criticality in extended $s = \frac{1}{2}$ Heisenberg models on the triangular lattice, *Phys. Rev. B* **95**, 035141 (2017).
 - [5] C. Hickey, L. Cincio, Z. Papić, and A. Paramekanti, Emergence of chiral spin liquids via quantum melting of noncoplanar magnetic orders, *Phys. Rev. B* **96**, 115115 (2017).
 - [6] L. Messio, S. Bieri, C. Lhuillier, and B. Bernu, Chiral spin liquid on a kagome antiferromagnet induced by the Dzyaloshinskii-Moriya interaction, *Phys. Rev. Lett.* **118**, 267201 (2017).
 - [7] S. Bieri, C. Lhuillier, and L. Messio, Projective symmetry group classification of chiral spin liquids, *Phys. Rev. B* **93**, 094437 (2016).
 - [8] W.-J. Hu, S.-S. Gong, and D. N. Sheng, Variational Monte Carlo study of chiral spin liquid in quantum antiferromagnet on the triangular lattice, *Phys. Rev. B* **94**, 075131 (2016).
 - [9] A. Wietek, A. Sterdyniak, and A. M. Läuchli, Nature of chiral spin liquids on the kagome lattice, *Phys. Rev. B* **92**, 125122 (2015).
 - [10] H. Yao and D.-H. Lee, Fermionic magnons, non-Abelian spinons, and the spin quantum Hall effect from an exactly solvable spin-1/2 Kitaev model with $SU(2)$ symmetry, *Phys. Rev. Lett.* **107**, 087205 (2011).
 - [11] J.-Y. Chen, J.-W. Li, P. Nataf, S. Capponi, M. Mambrini, K. Totsuka, H.-H. Tu, A. Weichselbaum, J. von Delft, and D. Poilblanc, Abelian $SU(N)_1$ chiral spin liquids on the square lattice, *Phys. Rev. B* **104**, 235104 (2021).
 - [12] M. Hermele, V. Gurarie, and A. M. Rey, Mott insulators of ultracold fermionic alkaline earth atoms: Underconstrained magnetism and chiral spin liquid, *Phys. Rev. Lett.* **103**, 135301 (2009).
 - [13] P. Nataf, M. Lajkó, A. Wietek, K. Penc, F. Mila, and A. M. Läuchli, Chiral spin liquids in triangular-lattice $SU(N)$ fermionic Mott insulators with artificial gauge fields, *Phys. Rev. Lett.* **117**, 167202 (2016).
 - [14] J.-Y. Chen, S. Capponi, A. Wietek, M. Mambrini, N. Schuch, and D. Poilblanc, $SU(3)_1$ chiral spin liquid on the square lattice: A view from symmetric projected entangled pair states, *Phys. Rev. Lett.* **125**, 017201 (2020).
 - [15] Y.-H. Zhang, D. N. Sheng, and A. Vishwanath, $SU(4)$ chiral spin liquid, exciton supersolid, and electric detection in moiré bilayers, *Phys. Rev. Lett.* **127**, 247701 (2021).
 - [16] X.-P. Yao, Y. Gao, and G. Chen, Topological chiral spin liquids and competing states in triangular lattice $SU(N)$ Mott insulators, *Phys. Rev. Res.* **3**, 023138 (2021).

- [17] G. Chen, K. R. A. Hazzard, A. M. Rey, and M. Hermele, Synthetic-gauge-field stabilization of the chiral-spin-liquid phase, *Phys. Rev. A* **93**, 061601(R) (2016).
- [18] M. Hermele and V. Gurarie, Topological liquids and valence cluster states in two-dimensional $SU(N)$ magnets, *Phys. Rev. B* **84**, 174441 (2011).
- [19] Y.-C. He, D. N. Sheng, and Y. Chen, Chiral spin liquid in a frustrated anisotropic kagome Heisenberg model, *Phys. Rev. Lett.* **112**, 137202 (2014).
- [20] W.-J. Hu, W. Zhu, Y. Zhang, S. Gong, F. Becca, and D. N. Sheng, Variational Monte Carlo study of a chiral spin liquid in the extended Heisenberg model on the kagome lattice, *Phys. Rev. B* **91**, 041124(R) (2015).
- [21] Y.-C. He and Y. Chen, Distinct spin liquids and their transitions in spin-1/2xxz kagome antiferromagnets, *Phys. Rev. Lett.* **114**, 037201 (2015).
- [22] S.-S. Gong, W. Zhu, L. Balents, and D. N. Sheng, Global phase diagram of competing ordered and quantum spin-liquid phases on the kagome lattice, *Phys. Rev. B* **91**, 075112 (2015).
- [23] S.-S. Gong, W. Zhu, and D. Sheng, Emergent chiral spin liquid: Fractional quantum Hall effect in a kagome Heisenberg model, *Sci. Rep.* **4**, 6317 (2014).
- [24] T. A. Sedrakyan, L. I. Glazman, and A. Kamenev, Spontaneous formation of a nonuniform chiral spin liquid in a moat-band lattice, *Phys. Rev. Lett.* **114**, 037203 (2015).
- [25] N. Y. Yao, M. P. Zaletel, D. M. Stamper-Kurn, and A. Vishwanath, A quantum dipolar spin liquid, *Nat. Phys.* **14**, 405 (2018).
- [26] A. Szasz, J. Motruk, M. P. Zaletel, and J. E. Moore, Chiral spin liquid phase of the triangular lattice Hubbard model: A density matrix renormalization group study, *Phys. Rev. X* **10**, 021042 (2020).
- [27] A. Kitaev, Anyons in an exactly solved model and beyond, *Ann. Phys. (NY)* **321**, 2 (2006).
- [28] H. Yao and S. A. Kivelson, Exact chiral spin liquid with non-Abelian anyons, *Phys. Rev. Lett.* **99**, 247203 (2007).
- [29] A. G. Grushin and C. Repellin, Amorphous and polycrystalline routes toward a chiral spin liquid, *Phys. Rev. Lett.* **130**, 186702 (2023).
- [30] V. Peri, S. Ok, S. S. Tsirkin, T. Neupert, G. Baskaran, M. Greiter, R. Moessner, and R. Thomale, Non-Abelian chiral spin liquid on a simple non-Archimedean lattice, *Phys. Rev. B* **101**, 041114(R) (2020).
- [31] M. A. Keskiner, O. Erten, and M. O. Oktel, Kitaev-type spin liquid on a quasicrystal, *Phys. Rev. B* **108**, 104208 (2023).
- [32] G. Cassella, P. d'Ornellas, T. Hodson, W. M. H. Natori, and J. Knolle, An exact chiral amorphous spin liquid, *Nat. Commun.* **14**, 6663 (2023).
- [33] V. Chua and G. A. Fiete, Exactly solvable topological chiral spin liquid with random exchange, *Phys. Rev. B* **84**, 195129 (2011).
- [34] V. Chua, H. Yao, and G. A. Fiete, Exact chiral spin liquid with stable spin fermi surface on the kagome lattice, *Phys. Rev. B* **83**, 180412(R) (2011).
- [35] J. Fu, Exact chiral-spin-liquid state in a Kitaev-type spin model, *Phys. Rev. B* **100**, 195131 (2019).
- [36] D. F. Schroeter, E. Kapit, R. Thomale, and M. Greiter, Spin Hamiltonian for which the chiral spin liquid is the exact ground state, *Phys. Rev. Lett.* **99**, 097202 (2007).
- [37] R. Thomale, E. Kapit, D. F. Schroeter, and M. Greiter, Parent Hamiltonian for the chiral spin liquid, *Phys. Rev. B* **80**, 104406 (2009).
- [38] M. Greiter, D. F. Schroeter, and R. Thomale, Parent Hamiltonian for the non-Abelian chiral spin liquid, *Phys. Rev. B* **89**, 165125 (2014).
- [39] S. Trebst and C. Hickey, Kitaev materials, *Phys. Rep.* **950**, 1 (2022).
- [40] Y. Kasahara, T. Ohnishi, Y. Mizukami, O. Tanaka, S. Ma, K. Sugii, N. Kurita, H. Tanaka, J. Nasu, Y. Motome, T. Shibauchi, and Y. Matsuda, Majorana quantization and half-integer thermal quantum Hall effect in a Kitaev spin liquid, *Nature (London)* **559**, 227 (2018).
- [41] M. Hermanns, I. Kimchi, and J. Knolle, Physics of the Kitaev model: Fractionalization, dynamic correlations, and material connections, *Annu. Rev. Condens. Matter Phys.* **9**, 17 (2018).
- [42] C. Kuhlenskamp, W. Kadow, A. Imamoğlu, and M. Knap, Chiral pseudospin liquids in moiré heterostructures, *Phys. Rev. X* **14**, 021013 (2024).
- [43] B.-Y. Sun, N. Goldman, M. Aidelsburger, and M. Bukov, Engineering and probing non-Abelian chiral spin liquids using periodically driven ultracold atoms, *PRX Quantum* **4**, 020329 (2023).
- [44] T.-H. Yang, B.-Z. Wang, X.-C. Zhou, and X.-J. Liu, Quantum Hall states for Rydberg arrays with laser-assisted dipole-dipole interactions, *Phys. Rev. A* **106**, L021101 (2022).
- [45] M. Kalinowski, N. Maskara, and M. D. Lukin, Non-Abelian Floquet spin liquids in a digital Rydberg simulator, *Phys. Rev. X* **13**, 031008 (2023).
- [46] S. Ohler, M. Kiefer-Emmanouilidis, and M. Fleischhauer, Quantum spin liquids of Rydberg excitations in a honeycomb lattice induced by density-dependent Peierls phases, *Phys. Rev. Res.* **5**, 013157 (2023).
- [47] S. Weber, R. Bai, N. Makki, J. Mögerle, T. Lahaye, A. Browaeys, M. Daghofer, N. Lang, and H. P. Büchler, Experimentally accessible scheme for a fractional chern insulator in Rydberg atoms, *PRX Quantum* **3**, 030302 (2022).
- [48] P. S. Tarabunga, G. Giudici, T. Chanda, and M. Dalmonte, Classification and emergence of quantum spin liquids in chiral Rydberg models, *Phys. Rev. B* **108**, 075118 (2023).
- [49] F. Verstraete and J. I. Cirac, Renormalization algorithms for quantum-many body systems in two and higher dimensions, *arXiv:cond-mat/0407066*.
- [50] F. Verstraete, M. M. Wolf, D. Perez-Garcia, and J. I. Cirac, Criticality, the area law, and the computational power of projected entangled pair states, *Phys. Rev. Lett.* **96**, 220601 (2006).
- [51] N. Schuch, I. Cirac, and D. Pérez-García, PEPS as ground states: Degeneracy and topology, *Ann. Phys. (NY)* **325**, 2153 (2010).
- [52] D. Poilblanc, J. I. Cirac, and N. Schuch, Chiral topological spin liquids with projected entangled pair states, *Phys. Rev. B* **91**, 224431 (2015).
- [53] D. Poilblanc, N. Schuch, and I. Affleck, $SU(2)_1$ chiral edge modes of a critical spin liquid, *Phys. Rev. B* **93**, 174414 (2016).
- [54] D. Poilblanc, Investigation of the chiral antiferromagnetic Heisenberg model using projected entangled pair states, *Phys. Rev. B* **96**, 121118(R) (2017).

- [55] S. Niu, J. Hasik, J.-Y. Chen, and D. Poilblanc, Chiral spin liquids on the kagome lattice with projected entangled simplex states, *Phys. Rev. B* **106**, 245119 (2022).
- [56] T. B. Wahl, H.-H. Tu, N. Schuch, and J. I. Cirac, Projected entangled-pair states can describe chiral topological states, *Phys. Rev. Lett.* **111**, 236805 (2013).
- [57] J. Dubail and N. Read, Tensor network trial states for chiral topological phases in two dimensions and a no-go theorem in any dimension, *Phys. Rev. B* **92**, 205307 (2015).
- [58] J. Hasik, M. Van Damme, D. Poilblanc, and L. Vanderstraeten, Simulating chiral spin liquids with projected entangled-pair states, *Phys. Rev. Lett.* **129**, 177201 (2022).
- [59] N. Schuch, D. Poilblanc, J. I. Cirac, and D. Pérez-García, Topological order in the projected entangled-pair states formalism: Transfer operator and boundary hamiltonians, *Phys. Rev. Lett.* **111**, 090501 (2013).
- [60] S. Yang, T. B. Wahl, H.-H. Tu, N. Schuch, and J. I. Cirac, Chiral projected entangled-pair state with topological order, *Phys. Rev. Lett.* **114**, 106803 (2015).
- [61] J.-Y. Chen, L. Vanderstraeten, S. Capponi, and D. Poilblanc, Non-Abelian chiral spin liquid in a quantum antiferromagnet revealed by an iPEPS study, *Phys. Rev. B* **98**, 184409 (2018).
- [62] A. E. B. Nielsen, G. Sierra, and J. I. Cirac, Local models of fractional quantum Hall states in lattices and physical implementation, *Nat. Commun.* **4**, 2864 (2013).
- [63] J. Yang, Z. Liu, and L. Wang, Ground state phase diagram and the exotic phases in the spin-1/2 square lattice J_1 - J_2 - J_χ model, [arXiv:2401.03434](https://arxiv.org/abs/2401.03434).
- [64] X.-T. Zhang, Y. Huang, H.-Q. Wu, D. N. Sheng, and S.-S. Gong, Chiral spin liquid and quantum phase diagram of spin-1/2 J_1 - J_2 - J_χ model on the square lattice, *Phys. Rev. B* **109**, 125146 (2024).
- [65] S. Niu, J.-W. Li, J.-Y. Chen, and D. Poilblanc, Chiral spin liquids with projected Gaussian fermionic entangled pair states, *Phys. Rev. B* **109**, L081107 (2024).
- [66] Y. Zhang, T. Grover, A. Turner, M. Oshikawa, and A. Vishwanath, Quasiparticle statistics and braiding from ground-state entanglement, *Phys. Rev. B* **85**, 235151 (2012).
- [67] Q. Mortier, N. Schuch, F. Verstraete, and J. Haegeman, Tensor networks can resolve fermi surfaces, *Phys. Rev. Lett.* **129**, 206401 (2022).
- [68] J.-W. Li, J. von Delft, and H.-H. Tu, $U(1)$ -symmetric Gaussian fermionic projected entangled paired states and their Gutzwiller projection, *Phys. Rev. B* **107**, 085148 (2023).
- [69] F. Becca and S. Sorella, *Quantum Monte Carlo Approaches for Correlated Systems* (Cambridge University Press, Cambridge, 2017).
- [70] H.-J. Liao, J.-G. Liu, L. Wang, and T. Xiang, Differentiable programming tensor networks, *Phys. Rev. X* **9**, 031041 (2019).
- [71] T. Nishino and K. Okunishi, Corner transfer matrix renormalization group method, *J. Phys. Soc. Jpn.* **65**, 891 (1996).
- [72] P. Corboz, T. M. Rice, and M. Troyer, Competing states in the t-J model: Uniform d-wave state versus stripe state, *Phys. Rev. Lett.* **113**, 046402 (2014).
- [73] Y. Zhang, T. Grover, and A. Vishwanath, Topological entanglement entropy of \mathbb{Z}_2 spin liquids and lattice Laughlin states, *Phys. Rev. B* **84**, 075128 (2011).
- [74] J.-W. Mei and X.-G. Wen, Modular matrices from universal wave-function overlaps in Gutzwiller-projected parton wave functions, *Phys. Rev. B* **91**, 125123 (2015).
- [75] X. G. Wen and Q. Niu, Ground-state degeneracy of the fractional quantum hall states in the presence of a random potential and on high-genus Riemann surfaces, *Phys. Rev. B* **41**, 9377 (1990).
- [76] L. Tarruell and L. Sanchez-Palencia, Quantum simulation of the hubbard model with ultracold fermions in optical lattices, *C. R. Phys.* **19**, 365 (2018).
- [77] X. Wang, E. Khatami, F. Fei, J. Wyrick, P. Namboodiri, R. Kashid, A. F. Rigosi, G. Bryant, and R. Silver, Experimental realization of an extended Fermi-Hubbard model using a 2d lattice of dopant-based quantum dots, *Nat. Commun.* **13**, 6824 (2022).
- [78] B. M. Spar, E. Guardado-Sanchez, S. Chi, Z. Z. Yan, and W. S. Bakr, Realization of a Fermi-Hubbard optical tweezer array, *Phys. Rev. Lett.* **128**, 223202 (2022).
- [79] A. Hackenbroich, A. Sterdyniak, and N. Schuch, Interplay of $SU(2)$, point group, and translational symmetry for projected entangled pair states: Application to a chiral spin liquid, *Phys. Rev. B* **98**, 085151 (2018).
- [80] J. I. Cirac, D. Poilblanc, N. Schuch, and F. Verstraete, Entanglement spectrum and boundary theories with projected entangled-pair states, *Phys. Rev. B* **83**, 245134 (2011).
- [81] W.-L. Tu, F. Schindler, T. Neupert, and D. Poilblanc, Competing orders in the hofstadter t-J model, *Phys. Rev. B* **97**, 035154 (2018).